ACERP: Vol. 2, No. 1 (Winter 2016) 32-37

Advanced Ceramics Progress

Research Article

Journal Homepage: www.acerp.ir

# Optimization of the Nano-Porous Silicon Structures by Magnesiothermic Reduction of the As-Synthesized Silica

M. Nangir, A. Massoudi*, R. Yazdanirad, S.A. Tayebifard

*Department of semiconductors, Materials and energy research center, Tehran, Iran.*

*PAPER INFO*

***Paper history:***
**Received** 23 February 2016
**Accepted in revised form** 18 June 2016

*Keywords*:
Nano-porous silicon,
magnesiothermic reduction,
nano-structured silica

*ABSTRACT*

Nano-porous silicon powders were produced via novel efficient magnesiothermic reduction. In this work, thermal and reduction process time effects on the porous silicon structure were investigated. The nano-porous silicon powders were characterized by X-ray diffraction analysis and field emission scanning electron microscopy. It was the first time that the nano-porous structure was produced in presence of both novel $SiO_2$ cryogel and $SiO_2$ nano-particles at heating ramp rate of 10 $^0$C/min and was changed to homogeneous and uniform porous structure throughout the sample when the heating ramp rate was controlled at 5 $^0$C/min. It was held that the wall thickness and average pore size of uniform porous silicon were decreased from 120.8 nm and 219.05 nm at the heating ramp rate of 10 $^0$C/min to 87.6 nm and 195.8 nm at heating ramp rate of 5 $^0$C/min, respectively.

## 1. INTRODUCTION

Silicon is second abundant element after oxygen in the earth. It is an important element because of its high melting point (1414$^0$C) and low density (2.32 g cm$^{-3}$). To date, silicon attracts many researchers attentions for its unique properties in semiconductors [1] and optoelectronic applications [2]. In addition, silicon nanostructures attract much attention as a promising nanostructure for high technology devices such as gas sensing [3], energy storage devices [4, 5] and biological applications [6]. Silicon nano-particles (SiNPs) are common nanostructures applicable in different industries [7]. To date, silicon nano-particles are produced by various chemical, physical and mechanical methods. Micro-emulsion synthesis is one of the popular methods for producing SiNPs [8]; Moreover, to this end researchers have used electrochemical reduction of silica precursor in presence of molten salt as a chemical route [9]. Gaseous compound pyrolysis was also used to produce SiNPs [10]. Furthermore, physical and mechanical methods such as low pressure microwave [11], ball mill [12] and Pulsed laser ablation (PLA) [13] were used for SiNPs synthesis.

Recently, many Si nanostructures such as quantum dots[14], Si nano-wires [15] and porous structures [16] attract much attention. On the other hand, electrochemical etch is a common technique for producing porous silicon (PSi) [17]. In this way, boron-doped Si wafer in presence of HF- based electrolyte etched under constant current density. Chemical etching is another method for producing etched PSi layer [18]. Investigation on porous silicon nano-powders was carried out by reducing $SiO_2$ with different precursors such as SBA-15[6], MCM-48 [19] and TEOS [20]. Moreover, $SiO_2$ cryogel with unique properties such as low density (more less than 0.05 g/cm$^3$) and 700-800 m$^2$/g specific surface area was produced by freeze drying method as an appropriate method to synthesize porous materials [21] that can be used as a source of porous Si. The diameter of pores in porous structure divided into three classes containing spongy micro-porous (pore size <10 nm), branchy meso-porous silicon (pore size 10–50 nm) and classical macro-porous silicon (pore size 50 nm–20 $\mu$m) [22].

Nano-porous structures are favorable structures because of their high porosities and high surface area [23]. So far, magnesiothermic reduction is a common method for producing nano-porous silicon [6, 24]. In this method, $SiO_2$ as a source of Si was reduced to nano-porous Si by magnesium as a reducing agent. Recently, Lu Shi and co-workers were used the bio-silica from the rice husks as the silica precursor and synthesized porous Si by magnesiothermic reduction method [25]. The advantage of this method in comparison to chemical methods is conservation of morphology of raw $SiO_2$, In addition this method has the advantage of low temperature and short

*Corresponding Author's Email: massoudi.a@merc.ac.ir (A. Massoudi)

process time in comparison to physical and mechanical methods respectively.

To date, synthesis of nano-porous silicon via magnesiothermic reduction are rapidly developed in the world. During recent years, produced silicon through this route are potentially used in a number of applications such as optoelectronic devices [21] and biomedical industry [6]. In addition, the synthesized nano-porous silicon are extensively investigated as a novel anode for rechargeable lithium-ion batteries [16].

In this work, we reported the synthesis of homogeneous porous structure of silicon via magnesiothermic reduction of both novel $SiO_2$ cryogel and $SiO_2$ nano-particles. The effects of changing several parameters such as heating ramp rate and heating process time on producing chemical composition and morphology have been investigated. It has shown that the heating ramp rate is an essential parameter which changes the morphology of nano-porous silicon.

## 2. EXPERIMENTAL

### 2.1. Materials

Raw materials used in this study were TEOS, HF, HCl, EtOH, $NH_4OH$ and Mg powder. Tetraethyl orthosilicate (TEOS, 99.98%, Merck, German), hydrofluoric acid (HF, 40%, Merck, German), hydrochloric acid (HCl, 37%, Merck, German) and absolute ethanol (EtOH, 97%, Merck, German) were used to produce Si nanostructures. Ammonium hydroxide ($NH_4OH$, 28%, Merck, German) was used to prepare the $SiO_2$ nano-particles. Magnesium powder (0.3mm, ≥98.5%, Merck) as a reducing agent was used for magnesiothermic processes.

### 2.2. Synthesis of $SiO_2$ Cryogel by Freeze Drying Method

To prepare $SiO_2$ cryogel, Ethanol (EtOH) and deionized (DI) water were mixed at room temperature. Hydrofluoric acid (HF), after tetraethyl orthosilicate (TEOS), was added to the mixture. The molar ratio of TEOS: EtOH: $H_2O$: HF was 1: 8: 4: 0.6. After stirring the mixture for several minutes, it was kept in static conditions for 20 minutes to form a uniform transparent gel. The gel sample was aged at room temperature in ethanol for 7 days. Finally, silica cryogel was successfully obtained by using freeze drying method. In this stage, the solvent was exchanged by DI water for 12 hours. Then, the gel was kept in freeze drying chamber for 24 hours after immerging into liquid nitrogen for 50 minutes. Figure 1 depicts the steps for producing $SiO_2$ cryogel.

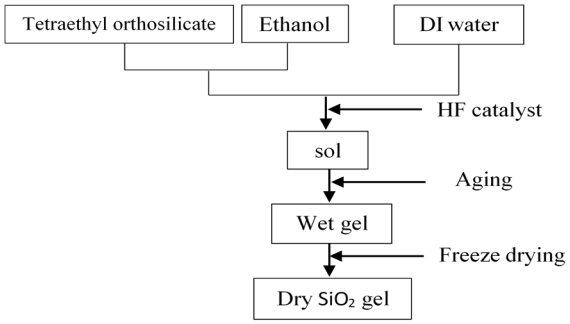


**Figure 1.** Schematic image of $SiO_2$ cryogel synthesis steps.

### 2.3. Synthesis of $SiO_2$ Nano-Particles by Stober Method

Silica nanoparticles were synthesized by hydrolysis of TEOS in presence of ammonium hydroxide. In this way, EtOH and deionized water were mixed and kept in a sonication bath. TEOS was added to the solution after 10 minutes. After 20 minutes 14 M $NH_4OH$ was added to the solvent and was kept for 75 minutes. All processes were done in ultrasonic bath. Molar ratio of TEOS: $NH_4OH$: EtOH: $H_2O$ was chosen 0.045: 14: 4: 14, respectively. $SiO_2$ nano-particles were subsequently obtained after heat treatment at $100^0$C for 3 hours.

### 2.4. Preparation of Porous Si via Magnesiothermic Reduction

To reduce $SiO_2$ to element silicon, $SiO_2$ and Mg powder were weighted in stoichiometry ratio and mixed. The molar ratio of $SiO_2$: Mg was 1:2.5. Samples were prepared through two ways, pellet and non-pellet. The pelletized samples were pressed under 423 Mpa pressure by SVO151G5-1 uniaxial cold press. The weight, diameter and thickness of each pellet were 0.8 g, 10 mm and 3mm, respectively. Afterward, the samples were placed in stainless steel container. The stainless steel container avoids local heat accumulation during the magnesiothermic reduction. The stainless steel container was moved to tubular furnace and heat treated under argon atmosphere. The mixture in furnace was heated to $670^0$C with a ramp rate of 10 $^0$C/min and 5 $^0$C/min, respectively. Samples were naturally cooled at room temperature. The process parameters used for synthesis are tabulated in table 1.

After reduction, the samples were leached in 1 M HCl solution for 24 hours and then 1 M HF solution for 20 minutes. The products were washed in deionized water and ethanol for several times. Finally, the produced porous Si was obtained after drying at 100 $^0$C for 2.5 hours.

**Table 1:** The conditions used to produce Si mesoporous by magnesiothermic reduction.

| No. | Sample | $SiO_2$ source | Reduction temp. (˚C) | Process time (h) | Rate (˚C/min) |
|---|---|---|---|---|---|
| 1 | Si-10G8-p | Gel | 670 | 8 | 10 |
| 2 | Si-10G4-p | Gel | 670 | 4 | 10 |
| 3 | Si-10NP4-p | Nano-particle | 670 | 4 | 10 |
| 4 | Si-10NP2.5-n | Nano-particle | 670 | 2.5 | 10 |
| 5 | Si-5NP2.5-n | Nano-particle | 670 | 2.5 | 5 |

In the sample column, silicon was called Si. After that, first number is the heating ramp rate, first letter is source of $SiO_2$, the second number is process time and the second letter is type of pellet. For instance, Si-10G8-p, Si: silicon, 10: 10 $^0$C/min, G: $SiO_2$ cryogel, 8: 8 hours and p: pellet.

### 2.5. Structure Characterization

The phase composition of samples were determined by a Phillips pw 3710 X-ray diffractometer with Co $K_\alpha$ radiation ($\lambda$=1.789010 $^0$A) at 0.02 $^0$/min in the 2$\theta$ ranges from $5^0$ to $85^0$. Field emission scanning electron microscopy (FESEM) (MIRA3 TESCAN model) and Energy dispersive X-ray spectroscopy (EDS) were carried out to observe samples morphology and identify chemical composition of samples, respectively.

## 3. RESULTS AND DISCUSSION

The melting point of magnesium is 650 $^0$C. When $SiO_2$ were mixed with Mg powder and heated, the redox reaction (1) occurs to produce porous Si [26].

$$SiO_{2(s)} + 2Mg_{(s)} \rightarrow 2MgO_{(s)} + Si_{(s)} \quad (1)$$
$$\Delta G_T^0 = -339.6$$
$$SiO_{2(s)} + 3MgO_{(l)} \rightarrow MgSiO_{3(s)} + 2MgO_{(s)} \quad (2)$$

In first reaction, the magnesium powder was used as a reducing agent and results in Si/MgO nano-composites production. The molten magnesium oxide reacts with $SiO_2$ and leads to $MgSiO_3$ and MgO products. The produced MgO was removed by acid leaching but $MgSiO_3$ still remains. The effects of parameters used in this study on synthesized pure homogeneous porous Si are as follows;

### 3.1. The Effect of $SiO_2$ Morphology

Figure 2 shows XRD patterns of synthesized Si at 670 $^0$C with a ramp rate of 10 $^0$C/min for 4 hours in presence of both cryogel and nano-particle structures of $SiO_2$. Figure 2-a depicts the board peak of amorphous $SiO_2$. In Figure 2-b and 2-c, the existence of the four peaks in 2$\theta$ = $33.10^0$, $55.48^0$, $66.13^0$ and $82.44^0$ were corresponding to (111), (220), (311) and (400) orientations. This orientations were shown in cubic silicon phase. The XRD patterns in Figure 2 suggest that $MgSiO_3$and $Mg_2Si$ were produced when $SiO_2$ nano-particle was used as source of Si (Si-10NP4-p sample). While, the pure Si was synthesized when $SiO_2$ cryogel was used as a source of Si (Si-10G4-p sample). $MgSiO_3$ is an unsolvable compound in HCl and HF solution. So, it was not removed by acid washing. Figure 3 shows the morphology of silica cryogel, silica nano-particles and synthesized porous Si after acid leaching. Figure 3-c depicts porous structure with particles agglomeration.

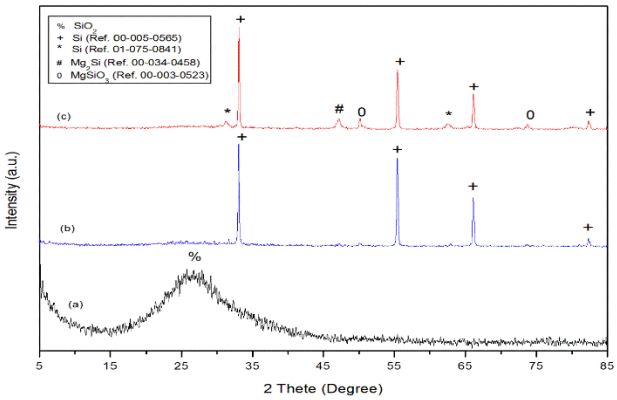


**Figure 2.** The XRD patterns of the obtained products after the magnesiothermic reduction. (a) $SiO_2$ amorphous, (b) Si-10G4-p sample, (c) Si-10NP4-p sample

While, Figure 3-d depicts porous structure with particles nucleation. Moreover, Figure 3-d legend depicts spongy-like porous structure. The measured average pore size was around 219.05 nm. Figure 3-e and 3-f also show X-ray energy dispersive (EDS) spectra of Si-10G4-p andSi-10NP4-p samples. The EDS spectra of both samples are consist of Si element but a little percent of Mg, F and O were observed in Si-10NP4-p sample due to the presence of $MgSiO_3$ and $Mg_2Si$.

### 3.2. The Effect of Reduction Time

Figure 4 shows the XRD pattern of synthesized Si at 670 $^0$C with a ramp rate of 10 $^0$C/min under 8, 4 and 2.5 hours heat treatment, respectively. The comparison of three patterns shows that the increasing of reduction process time has no effect on product crystallite phase. Figure 5 depicts FESEM macrograph of produced Si at 670 $^0$C in three different reduction times. Once the reaction time was 8 hours, the meso-porous structure was formed (Figure 5-a). Moreover, particles agglomeration was clearly observed. In Figure 5-b, macrograph of Si-10NP4-p sample are shown. The porous structure could be easily observed Figure 5-b also demonstrates Si particles which are germinated on surface of porous structure but was not grow because of short process time. The minimum, maximum and average pore size was measured to be 105.62 nm, 396.9 nm and 219.05 nm,

respectively. While, in Figure 5-c, the formation of macro-porous structure could be observed as a result of reduction in of process time to 2.5 hours. The minimum, maximum and average pore size of Si-10NP2.5-n sample was measured to be 120 nm, 282 nm and 214.3 nm, respectively. Therefore, by reducing the reduction time from 8 hours to 2.5 hours, the produced meso-porous structure changes to macro-porous structure. Furthermore, decreasing the process time from 4 hours to 2.5 hours lets to the forming of the smaller pore size. Figure 5-e to 5-g also shows X-ray energy dispersive (EDS) spectra of Si-10G8-p, Si-10NP4-p and Si-10NP2.5-p samples.

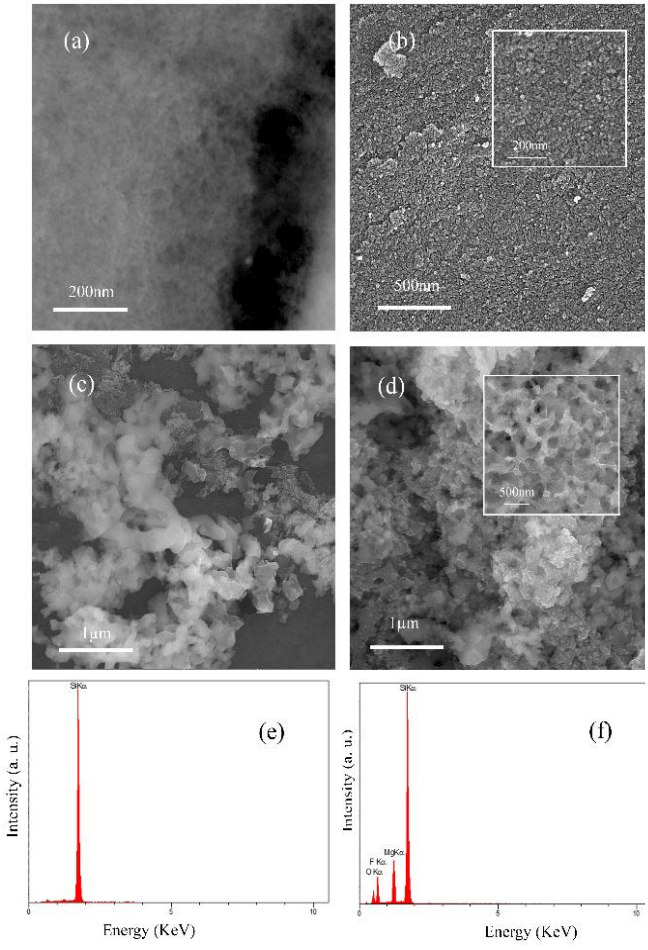


**Figure 2.** FESEM macrograph of (a) $SiO_2$ cryogel, (b) $SiO_2$ nanoparticles, (c) Si-10G4-p sample, (d) Si-10NP4-p sample and X-ray energy dispersive (EDS) spectra of (e) Si-10G4-p and (f) Si-10NP4-p. Sub-Figure b depicts $SiO_2$ nanoparticles in magnification of 200 nm. Sub-Figure d depicts spongy-like porous structure in magnification of 500 nm.

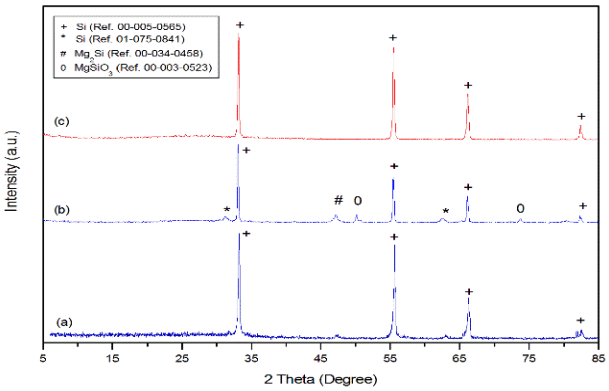


**Figure 3.** The XRD patterns of the obtained products after the magnesiothermic reduction. (a) Si-10G8-p sample, (b) Si-10NP4-p sample, (c) Si-10NP2.5-n sample.

### 3.3. The Effect of Heating Ramp Rate

Figure 6 shows XRD patterns of synthesized porous Si at 670 $^0$C with two heating ramp rate of 10 $^0$C/min and 5$^0$C/min. In both patterns the cubic silicon phase without any impurity was synthesized. Figure 7 depicts FESEM macrographs of Si-10NP2.5-n and Si-5NP2.5-n samples. During magnesiothermic reduction of $SiO_2$ to Si, it was found that the ramp rate was significantly affects the produced silicon powder morphology. The heterogeneous porosity with a wall thickness of 120.8 nm and average pore size of 219.05 nm was formed when the ramp rate was 10 $^0$C/min. When the ramp rate was controlled at 5 $^0$C/min, the homogeneous porous with honeycomb-like structure with uniform porosity was observed. The uniform and homogeneous porous structure throughout the sample is depicted in Figure 7-c. Moreover, a wall thickness and average pore size were decreased to 87.6 nm and 195.8 nm, respectively representing a high porosity of silicon powder.

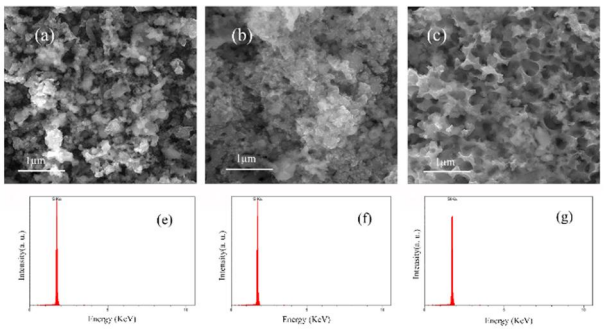


**Figure 4.** FESEM macrograph of synthesized Si products via magnesiothermic reduction with a ramp rate of 10 $^0$C/min for 8, 4 and 2.5 hours. (a) Si-10G8-p, (b) Si-10NP4-p, (c) Si-10NP2.5-p.

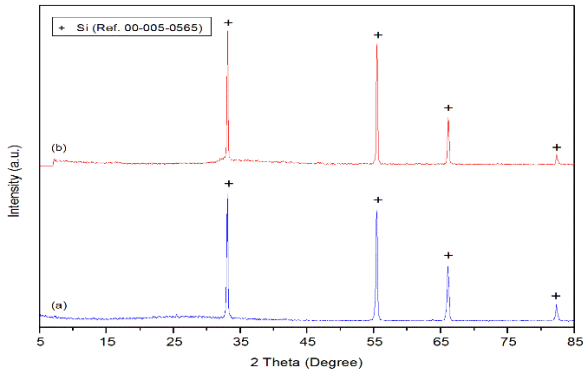


**Figure 5.** The XRD patterns of the obtained products after the magnesiothermic reduction. (a) Si-10NP2.5-n sample, (b) Si-5NP2.5-n sample.

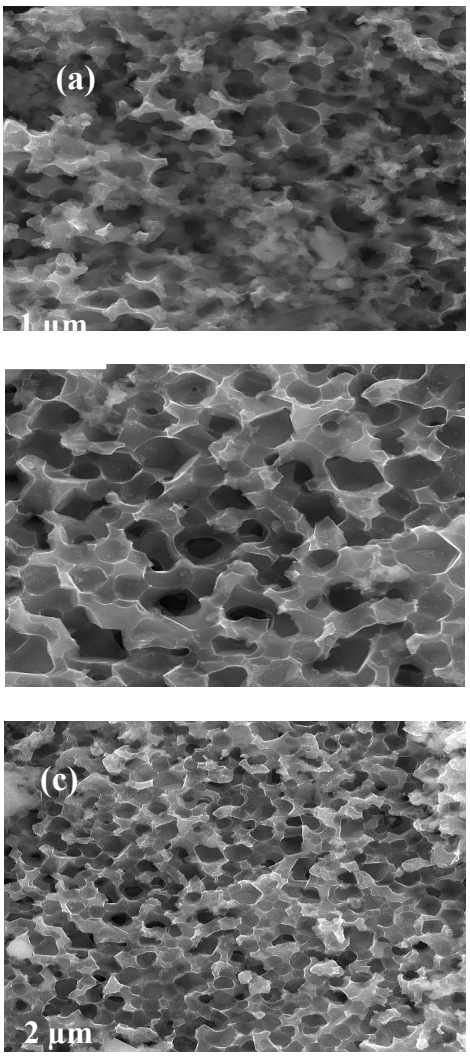


**Figure 6.** FESEM macrograph of synthesized Si products via magnesiothermic reduction with a ramp rate of (a) 10 $^0$C/min in Si-10NP2.5-p sample and (b) 5 $^0$C/min in Si-5NP2.5-p sample for 2.5 hours. Figure c depicts homogeneous porosity throughout the Si-5NP2.5-p sample in magnification of 2 µm.

## 4. CONCLUSION

In summary, 3D porous silicon with uniform porosity was successfully synthesized via magnesiothermic reduction method. The porous structure was produced by both $SiO_2$ cryogel and nano-particles precursor materials. Moreover, decreasing heating time to 2.5 hours results in production of macroporous silicon powder and $MgSiO_3$ by product removal. The Si products at 10 $^0$C/min heating rate show macroporous structure with average pore size of 219.05 nm, While, magnesiothermic reduction with ramp rate of 5 $^0$C/min led to uniform and homogenous porosity with 195.8 nm average pore size.

## 5. ACKNOWLEDGEMENT

The authors acknowledge the Materials and Energy Research Center (MERC) for funding this research.

## REFERENCE

1. Kuen-Hsien. Wu, Chong-Wei. Li, Jung-Hsuan. Liu, "Large enhancement of ultra-violet photoresponse of silicon-nanoparticle-embedded porous silicon thin films by rapid-thermal-oxidation treatment", ***Microelectronic Engineering***, vol. 148, (2015), 70-73.
2. Conibeer. G, Green. M, Cho. E- H, König. D, Cho. Y- H, Fangsuwannarak. T, Scardera. G, Pink. E, Huang. Y, Puzzer. T, "Silicon quantum dot nanostructures for tandem photovoltaic cells", ***Thin Solid Films***, vol. 516, (2008), 6748-6756.
3. Naderi. N, Hashim. M, Amran. T, "Enhanced physical properties of porous silicon for improved hydrogen gas sensing", ***Superlattices and Microstructures***, vol. 51, (2012), 626-634.
4. Zhou. Y, Jiang. X, Chen. L, Yue. J, Xu. H, Yang. J, Qian. Y, "Novel mesoporous silicon nanorod as an anode material for lithium ion batteries", ***Electrochimica Acta***, vol. 127, (2014), 252-258.
5. Yan. D, Bai. Y, Yu. C, Li. X, Zhang. W, "A novel pineapple-structured Si/TiO 2 composite as anode material for lithium ion batteries", ***Journal of Alloys and Compounds***, vol. 609, (2014), 86-92.
6. Guo. M, Zou. X, Ren.H, Muhammad. F, Huang.C, Qiu. S, Zhu.G, "Fabrication of high surface area mesoporous silicon via magnesiothermic reduction for drug delivery", ***Microporous and Mesoporous Materials***, vol. 142, (2011), 194-201.
7. Huan. C, Shu-Qing. S, "Silicon nanoparticles: Preparation, properties, and applications", ***Chinese Physics B***, vol. 23, (2014), 088102.
8. Liong. W, Sreekantan. S, Hutagalung. S. D, "Effect of concentration of sodium borohydrate on the synthesis of silicon nanoparticles via microemulsion routee", ***World Academy of Science, Engineering and Technology***, vol. 59, (2009), 419-422.

9. Nohira. T, Yasuda. K, Ito. Y, "Pinpoint and bulk electrochemical reduction of insulating silicon dioxide to silicon", ***Nature materials***, vol. 2. (2003). 397-401.
10. Li. X, He. Y, Swihart. M. T, "Surface functionalization of silicon nanoparticles produced by laser-driven pyrolysis of silane followed by HF-HNO3 etching", ***Langmuir***, vol. 20, (2004), 4720-4727.
11. Knipping. J, Wiggers. H, Rellinghaus. B, Roth. P, Konjhodzic. D, Meier. C, "Synthesis of high purity silicon nanoparticles in a low pressure microwave reactor", ***Journal of nanoscience and nanotechnology***, vol. 4, (2004), 1039-1044.
12. Leblanc. D, Hovington. P, Kim. C, Guerfi. A, Bélanger. D, Zaghib. K, "Silicon as anode for high-energy lithium ion batteries: From molten ingot to nanoparticles", ***Journal of Power Sources***, vol. 299, (2015), 529-536.
13. Odachi. G, Sakamoto. R, Hara. K, Yagi. T, "Generation of nanoparticles at a fluence less than the ablation threshold using femtosecond laser pulses", ***Applied Surface Science***, vol. 282, (2013), 638-641.
14. Cho. E.-C., Park. S, Hao. X, Song. D, Conibeer. G, Park. S.-C., Green. M.A, "Silicon quantum dot/crystalline silicon solar cells", ***Nanotechnology***, vol. 19(24), (2008), 245201.
15. Bai. F, Li. M, Song. D, Yu. H, Jiang. B, Li. Y, "Metal-assisted homogeneous etching of single crystal silicon: A novel approach to obtain an ultra-thin silicon wafer", ***Applied Surface Science***, vol. 273, (2013), 107-110.
16. Ge. M, Fang. X, Rong. J, Zhou. C, "Review of porous silicon preparation and its application for lithium-ion battery anodes", ***Nanotechnology***, vol. 24, (2013), 422001.
17. Naderi. N, Hashim. M, "A combination of electroless and electrochemical etching methods for enhancing the uniformity of porous silicon substrate for light detection application", ***Applied Surface Science***, vol. 258, (2012), 6436-6440.
18. Zhang. M.-L, Peng. K.-Q, Fan. X, Jie. J.-S, Zhang. R.-Q, Lee. S.-T, Wong. N.-B, "Preparation of large-area uniform silicon nanowires arrays through metal-assisted chemical etching", ***The Journal of Physical Chemistry C***, vol. 112, (2008), 4444-4450.
19. Nishiyama. N, Park. D.H, Koide. A, Egashira. Y, Ueyama. K, "A mesoporous silica (MCM-48) membrane: preparation and characterization", ***Journal of Membrane Science***, vol. 182, (2001), 235-244.
20. Rao. K.S, El-Hami. K, Kodaki. T, Matsushige. K, Makino. K, "A novel method for synthesis of silica nanoparticles", ***Journal of Colloid and Interface Science***, vol. 289, (2005), 125-131.
21. Wong. D.P, Lien. H.-T, Chen. Y.-T, Chen. K.-H, Chen. L.-C, "Patterned growth of nanocrystalline silicon thin films through magnesiothermic reduction of soda lime glass", ***Green Chemistry***, vol. 14, (2012), 896-900.
22. Kumar. P, Huber. P, "Effect of etching parameter on pore size and porosity of electrochemically formed nanoporous silicon", ***Journal of Nanomaterials***, vol. 2007, (2007).
23. Canham. L, "Porous Silicon Formation by Porous Silica Reduction", Handbook of Porous Silicon, ***Springer***, 2014, pp. 85-92.
24. Jia. H, Gao. P, Yang. J, Wang. J, Nuli. Y, Yang. Z, "Novel Three-Dimensional Mesoporous Silicon for High Power Lithium-Ion Battery Anode Material", ***Advanced Energy Materials***, vol. 1, (2011), 1036-1039.
25. Shi. L, Wang. W, Wang. A, Yuan. K, Yang. Y, "Understanding the impact mechanism of the thermal effect on the porous silicon anode material preparation via magnesiothermic reduction", ***Journal of Alloys and Compounds***, vol. 661, (2016), 27-37.
26. Niyomwas. S, "Synthesis and characterization of silicon-silicon carbide composites from rice husk ash via self-propagating high temperature synthesis", ***Journal of Metals, Materials and Minerals***, vol. 19, (2009), 21-25.